Direct Fabrication of Highly Nanoporous Polystyrene Fibers via Electrospinning

Jinyou Lin,[†,ǂ,§] Bin Ding,[*,†,ǂ,§] Jianyong Yu,[ǂ] and Youlo Hsieh[*,||]

State Key Laboratory for Modification of Chemical Fibers and Polymer Materials, College of Materials Science and Engineering, Donghua University, Shanghai 201620, China, Nanomaterials Research Center, Modern Textile Institute, Donghua University, Shanghai 200051, China, College of Textiles, Donghua University, Shanghai 201620, China, and Fibers and Polymer Science, University of California, Davis, California 95616

ABSTRACT A direct approach for fabricating nanoporous polymer fibers via electrospinning has been demonstrated. Polystyrene (PS) fibers with micro- and nanoporous structures both in the core and/or on the fiber surfaces were electrospun in a single process by varying solvent compositions and solution concentrations of the PS solutions. The porous structures of the fibrous mats were characterized by field emission scanning electron microscopy and Brunauer–Emmett–Teller measurements to confirm that they could be accurately controlled by tuning vapor pressure of tetrahydrofuran (THF) and *N*,*N*-dimethylformamide (DMF) solvent mixtures and PS concentrations in the solutions. As the solution concentration decreased, the average fiber diameter decreased, whereas the bead density increased dramatically to show a beads-on-string morphology. Both the specific surface area and pore volume of the fibrous mats showed a unimodal distributions centered at 1/3 THF /DMF mix ratio. Fibers formed from 5 wt % PS in the 1/3 THF and DMF mixtures had the largest specific surface area of 54.92 $m^2 g^{-1}$ and a pore volume of 0.318 $cm^3 g^{-1}$, respectively.

KEYWORDS: electrospinning • nanoporous fibers • polystyrene • solvent evaporation • phase separation

INTRODUCTION

Electrospinning is a well recognized and effective technique to produce fibers with diameters in the micrometers down to tens of nanometers from the electrostatically driven jets of polymer solution or melts (1, 2). Many unique qualities that include intrinsically high specific surface area as a result of the small sizes of electrospun fibers have drawn interests in research for potential applications in diverse fields. The attempt to further increase the specific surface area by introducing porosity in the already fine fibers has shown to enhance performance in tissue engineering (3), filtration (4), catalysis (5), superhydrophobic surfaces (6, 7), drug delivery system (8), sensors (9, 10), dye-sensitized solar cells (11), etc.

Porosity in electrospun polymer fibers has been demonstrated, often involving the use of high vapor pressure solvents (12–15) or the inclusion of additives in the solutions (16–19) followed by their removal in postelectrospinning processes. Porous structure features on the fiber surfaces have been observed when fibers electrospun from solvents with high vapor pressure (12–15). In this approach, the pore sizes and size distribution could be adjusted via tuning the relative humidity (14). Using polymer mixtures that phase separate followed by removal of the discrete domains also generated porous fibers (16, 17). Addition of salts into an electrospinning system was another way to control the fiber structure and properties (18, 19). For example, Gupta et al. (19) reported that porous nylon-6 fibers could be obtained from removal of gallium trichloride ($GaCl_3$) Lewis acid–base complexation in nylon-6 via electrospinning. Highly porous fibers could also be obtained by sublimation of the solvent by solidifying the solvent-ladden fibers on cryogenically cooled collector followed by vacuum drying (20). Although these approaches are feasible, all require additional postelectrospinning treatment process, and in some cases complete removal of the unwanted components may be very difficult.

To the best of our knowledge, few have reported the preparation of electrospun nanoporous fibers possessing ultrahigh specific surface area without any post-treatment.

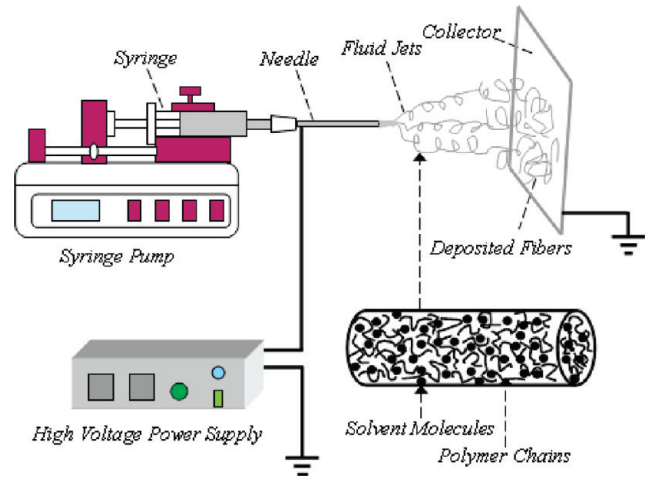

FIGURE 1. Schematic diagram of the electrospinning setup.

* To whom correspondence should be addressed. E-mail: binding@dhu.edu.cn; ylhsieh@ucdavis.edu.
Received for review October 27, 2009 and accepted January 22, 2010
† College of Materials Science and Engineering, Donghua University.
ǂ Modern Textile Institute, Donghua University.
§ College of Textiles, Donghua University.
|| University of California.
DOI: 10.1021/am900736h
© 2010 American Chemical Society

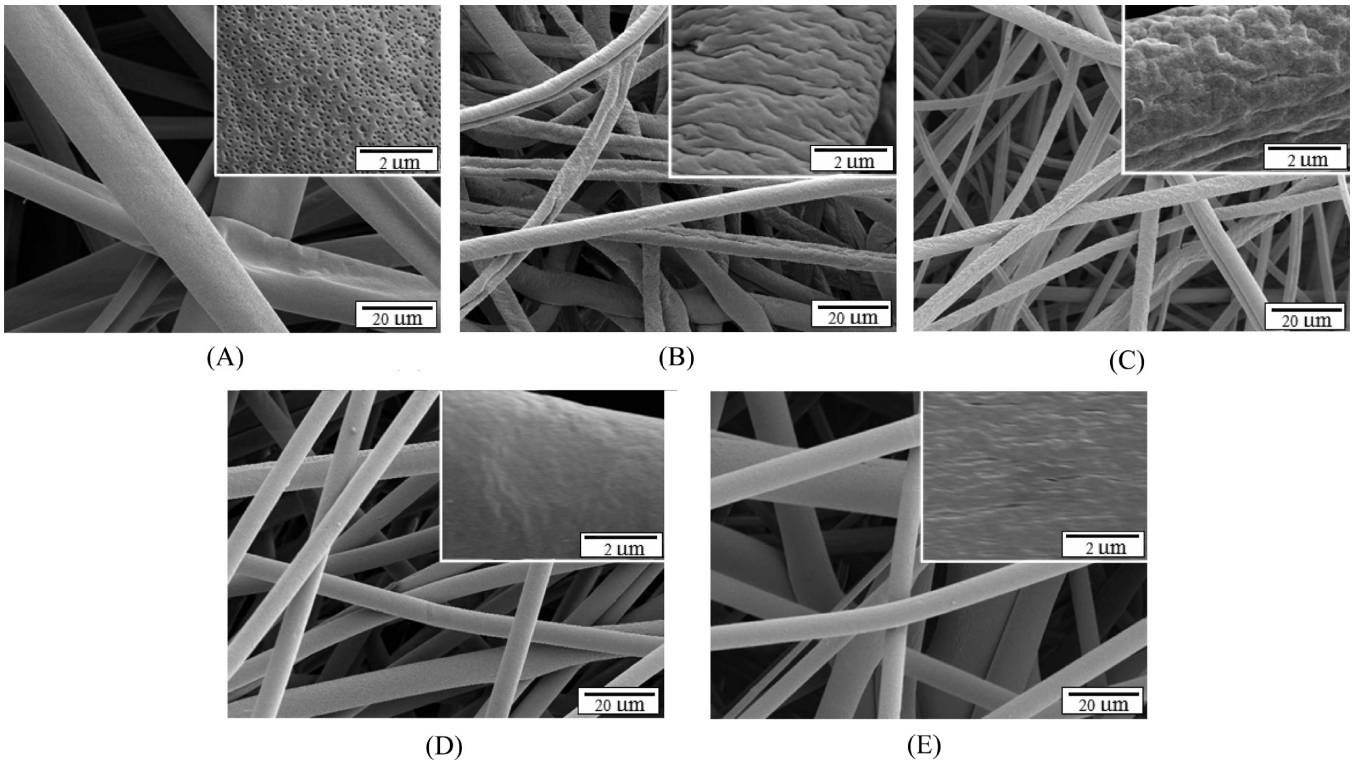

FIGURE 2. FE-SEM images of the PS fibers electrospun from 30 wt % PS solutions with different weight ratios of THF/DMF: (A) 4/0, (B) 3/1, (C) 2/2, (D) 1/3, and (E) 0/4.

In this study, we report an efficient and simple approach to prepare highly porous PS fibers directly via electrospinning PS solutions with various solvent compositions and polymer concentrations. PS was dissolved in the solvent mixtures of tetrahydrofuran (THF) with high vapor pressure and *N*,*N*-dimethylformamide (DMF) with low vapor pressure. The effects of the solvent compositions and polymer concentrations on the characteristics of as-spun fibers such as specific surface area, pore size, and pore distribution were intensively investigated.

EXPERIMENTAL SECTION

Materials. The polymer PS used in this study was purchased from Aldrich. The weight-average molecular weight (M_w) is 350,000 g/mol. Tetrahydrofuran (THF, Bp ≈ 66 °C, Vp at 25 °C ≈ 21.6 kPa, η/20 °C ≈ 0.468 mPa · s) and *N*,*N*-dimethylformamide (DMF, Bp ≈ 153 °C, Vp at 25 °C ≈ 2.7 kPa, η/20 °C ≈ 0.920 mPa s) (21) were purchased from EM Science and used as received. PS solutions were prepared at concentrations of 5, 10, 20, and 30 wt % by using mixture of solvents THF and DMF with various weight ratios of 4/0, 3/1, 2/2, 1/3, and 0/4, respectively.

Electrospinning. Figure 1 shows a schematic of the electrospinning setup employed in this work. The PS solution was placed in a syringe connected with a metal needle that was controlled by a syringe pump (Model 780200, KD Scientific) at a constant flow rate 2 mL/h. A high voltage power supply (Gamma High Voltage Supply, ES 30−0.1 P) was used to generate a potential difference of 20 kV between the needle and an aluminum grounded target placed 15 cm from the tip of the needle. All the experiments were carried out at 25 °C with the relative humidity of 40%.

Characterization. The viscosity and conductivity of polymer solutions were determined by using Rotational Viscometer (NDJ-79, Shanghai Changji Geological Instruments Co., China) and Mettler-Toledo Conductivity Meter (FE30, Switzerland), respectively. The morphology of the electrospun PS fibrous mats was observed by a field emission scanning electron microscopy (FE-SEM) (S-4800, Hitachi Ltd., Japan). The diameters of fibers were measured using an image analyzer (Adobe Photoshop CS2 9.0). The Brunauer−Emmett−Teller (BET) surface area, pore volume, and pore width of the fibrous mats were characterized by nitrogen adsorption using a surface area and porosity analyzer (Micromeritics, ASAP 2020).

RESULTS AND DISCUSSION

The FE-SEM images of fibers electrospun from 30 wt % PS solutions of various solvent compositions showed all fiber diameters to be in micrometer range (Figure 2) as be expected from the high polymer concentration. The average fiber diameters were 11.58, 6.17, 3.87, 6.63, and 5.78 μm from solvents at 4/0, 3/1, 2/2, 1/3, and 0/4 THF/DMF weight ratios, respectively (Table 1). The fibers electrospun from THF alone displayed a ribbon-like shape with densely packed nanopores on the fiber surfaces (Figure 2A). In mixed solvent with 25% DMF, the surface nanopores disappeared but wrinkled surface emerged (Figure 2B). Fibers electrospun from the equal THF and DMF mixture appeared irregularly coarse on the surfaces (Figure 2C). With further increased DMF in the solvent mixtures, the fiber surfaces became smooth (Figures 2D,E). The presence of surface nanopores appeared only on fibers electrospun from the high vapor pressure THF. With added DMF, the decreased vapor pressure slowed solvent evaporation. Decreasing of solvent evaporation from the jets allowed the charged jets to remain fluid, to continue to elongate, and the collapse resulting from atmosphere pressure and electrical repulsion reduced. It has been reported that highly volatile solvent utilized in electro-

Table 1. Fiber Diameter, Pore Volume, and Specific Surface Area of Electrospun PS Fibers

sample	fiber diameter (μm)	pore volume ($cm^3\ g^{-1}$)	specific surface ($m^2\ g^{-1}$)
30 wt % PS/THF	11.58 ± 5.44	0.004	0.98
30 wt % PS/(THF/DMF=3/1)	6.17 ± 1.16	0.006	1.10
30 wt % PS/(THF/DMF=2/2)	3.87 ± 1.21	0.007	1.05
30 wt % PS/(THF/DMF=1/3)	6.63 ± 0.85	0.092	14.18
30 wt % PS/DMF	5.87 ± 1.64	0.032	8.46
20 wt % PS/THF	3.14 ± 1.05	0.004	0.87
20 wt % PS/(THF/DMF=3/1)	3.58 ± 0.59	0.006	1.34
20 wt % PS/(THF/DMF=2/2)	3.05 ± 0.45	0.061	11.42
20 wt % PS/(THF/DMF=1/3)	2.52 ± 0.92	0.106	26.23
20 wt % PS/DMF	1.80 ± 0.47	0.067	12.23
10 wt % PS/THF		0.006	0.39
10 wt % PS/(THF/DMF=3/1)		0.024	8.93
10 wt % PS/(THF/DMF=2/2)		0.117	28.65
10 wt % PS/(THF/DMF=1/3)		0.182	48.37
10 wt % PS/DMF		0.119	37.77
5 wt % PS/(THF/DMF=1/3)		0.312	54.92

spinning could create nanopores on the fibers surface and the wrinkled surface resulted from buckling instabilities during processing (12, 22).

The cross-sectional FE-SEM images showed all PS fibers electrospun from 30 wt % PS solutions with various solvent compositions to have porous cores and thin sheaths of varying surface structures as described before (Figure 3). The pores in the cores appeared to increase in sizes with increasing DMF in the solvent mixtures. In the fibers formed from 1/3 THF/DMF (Figure 3D), the porous core seemed to consist of nanofibrils aligned along the fiber axis. Such alignment was obviously associated with high longitudinal strain rate of jet in electrospinning.

Such porous structures are expected to contribute to higher specific surface area of these PS fibers. The specific surface area and pore volume derived from BET measurements illustrated significant effects of the varied solvent compositions even there are no too much differences in their fiber diameters (Table 1). It could be observed that the fibrous mats formed from THF showed the lowest specific surface area of 0.98 $m^2\ g^{-1}$ and pore volume of 0.004 $cm^3\ g^{-1}$ because of its low pore volume below 200 nm (Figure 4 and Table 1), whereas that from DMF showed a 8.6 times of specific surface area (8.46 $m^2\ g^{-1}$) and nearly 8 times of pore volume (0.032 $cm^3\ g^{-1}$). Most intriguing is the even more impressive 14.18 $m^2\ g^{-1}$ specific surface area and

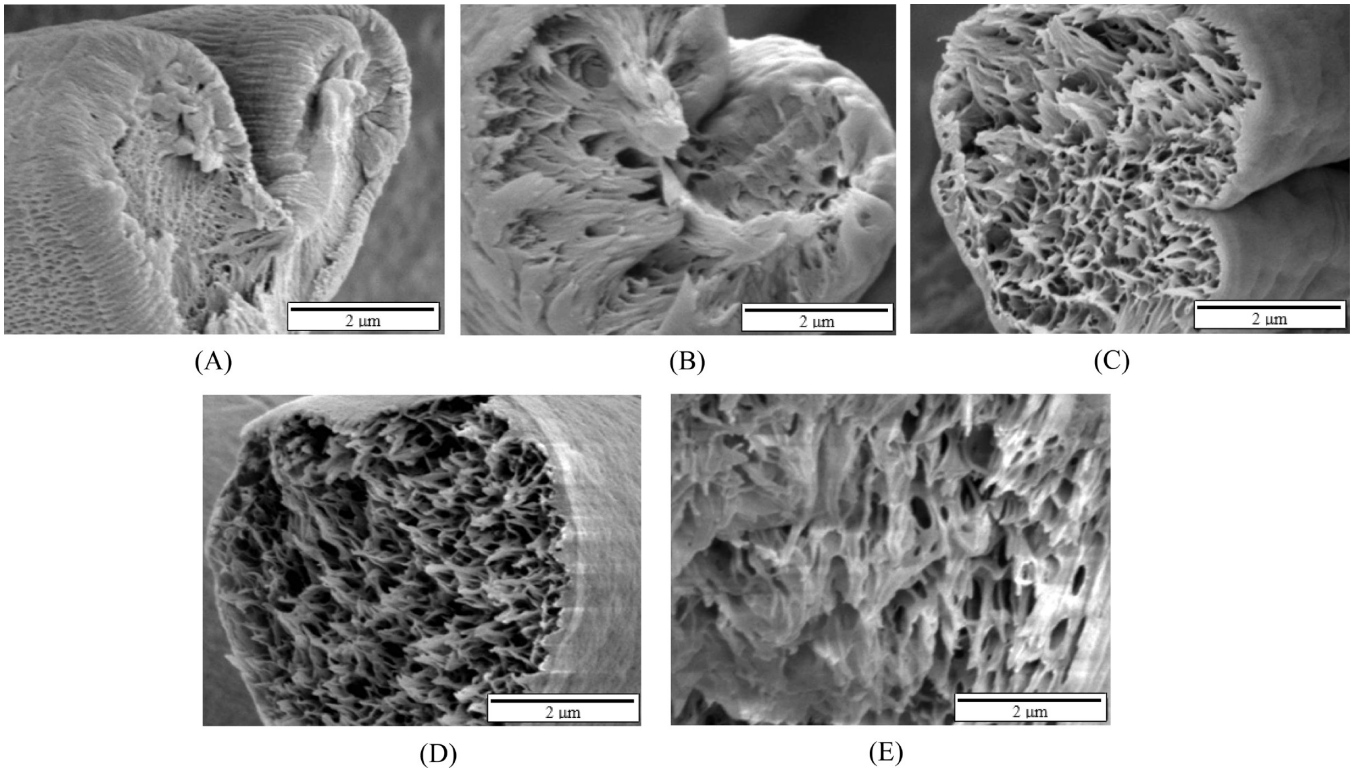

FIGURE 3. Cross-sectional FE-SEM images of PS fibers electrospun from 30 wt % PS solutions with different weight ratios of THF/DMF: (A) 4/0, (B) 3/1, (C) 2/2, (D) 1/3, and (E) 0/4.

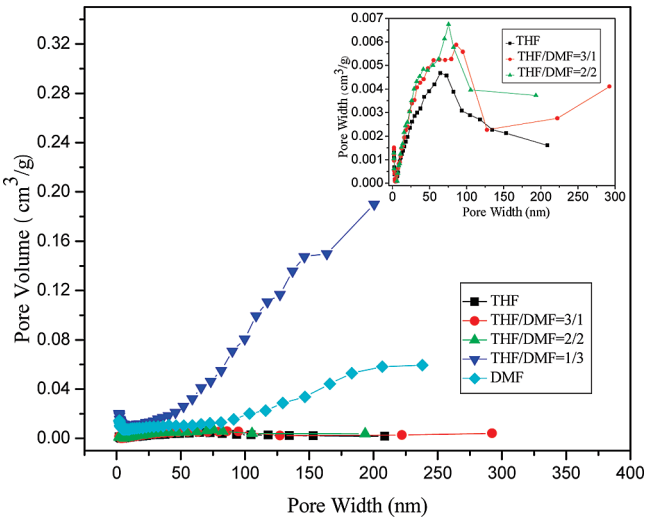

FIGURE 4. The pore size distribution for PS fibrous mats electrospun from 30 wt % PS solutions with different weight ratios of THF/DMF.

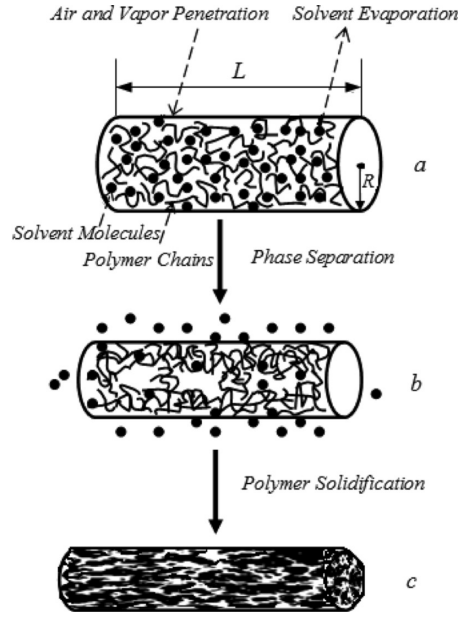

FIGURE 5. Schematic representation of the electrospun nanoporous fiber evolution process.

0.092 $cm^3\ g^{-1}$ pore volume of fibrous mats from the 1/3 THF/DMF mixture, or 15 and 23 fold higher, respectively. Although the decrease in fiber diameter is a factor to increase the fiber surface area, it can be concluded from the current results that the increase of PS fiber surface area is mainly caused by the formation of pores.

The mechanism of porous structure formation in electrospun fibers is very complex. A schematic representation of the evolution process of pore formation in electrospun fibers is shown in Figure 5. In carrying out electrospinning in an air environment (as nonsolvent), a cylindrical polymer fluid jet initially consisted of polymer chains and solvent molecules. Simultaneous diffusion processes of solvent evaporation outward and air vapor penetration inward occur at the jet skin-air interface (Figure 5(a)). The solvent removed from the polymer fluid jets involves the flash vaporization at the fiber surface and the diffusion from core to surface (23).

Table 2. Viscosity and Conductivity of the PS Solutions in THF/DMF with a Weight Ratio of 1/3 at Different Concentrations

PS concentration (wt %)	viscosity (mPa s)	conductivity (μs/cm)
5	5.8	8.86
10	21	4.47
20	242	2.91
30	1850	1.56

Flash vaporization of the solvent occurs when the fluid jets ejected from Taylor cone as a result of decompression of the polymer solution. This is accompanied by cooling from the consumption of the heat of vaporization, bringing the fluid jets to compositions and temperatures quite different from the original solution, leading to thermodynamically unstable jets and phase separation into polymer-rich and solvent-rich domains via binodal and/or spinodal decomposition (12) (Figure 5b).

As the solvent evaporated in combination with high fiber stretching under the electrical force, the concentrated polymer-rich phase solidified into the matrix, whereas the solvent-rich phase eventually transformed into the pores as solvent dried out (Figure 5c). The solidification effect has shown to be quickened from the increasing glass-transition temperature of the polymer solution because of solvent removal (24).

As the vapor pressure of the solvent mixture decreases with increasing DMF contents, the fluid jet solidification rate is slowed by the lowered solvent evaporation rate. The pore formation and pore sizes appear to highly depend on the relative rates of spinodal decomposition and solvent evaporation or jet solidification. Faster solidification of high vapor pressure solvent is capable of preserving the initial polymer-rich phase and solvent-rich phase, resulting in nanoporosity, whereas decreasing vapor pressure allows further phase separation when coupled with electrical force stretching and repulsion to create larger scale pore structures with smooth surfaces (Figures 2 and 3).

Previous studies have indicated the thermally induced phase separation and vapor-induced phase separation to be the main reasons for pores formation on the fiber surfaces (14, 25). The above observations clearly showed that the vapor pressure of the solvent mixtures plays critical role on the porous structure formation. Furthermore, the stretching arising from electrical force appears to be an important factor for inducing phase separation, especially for phase separation results preservation.

To demonstrate these further, fibers were electrospun from 20 wt % PS in the same series of solvent mixtures (Figure 6). All PS fibers were smaller than those electrospun from a higher 30 wt % PS concentration. Lowering the PS concentration is expected to decrease viscosity and increase conductivity (Table 2), which could accelerate jet and fiber stretching and result in the formation of thinner fibers (Table 1).

These pores were deformed and oriented along the fiber axis because of more intensive stretching arising from

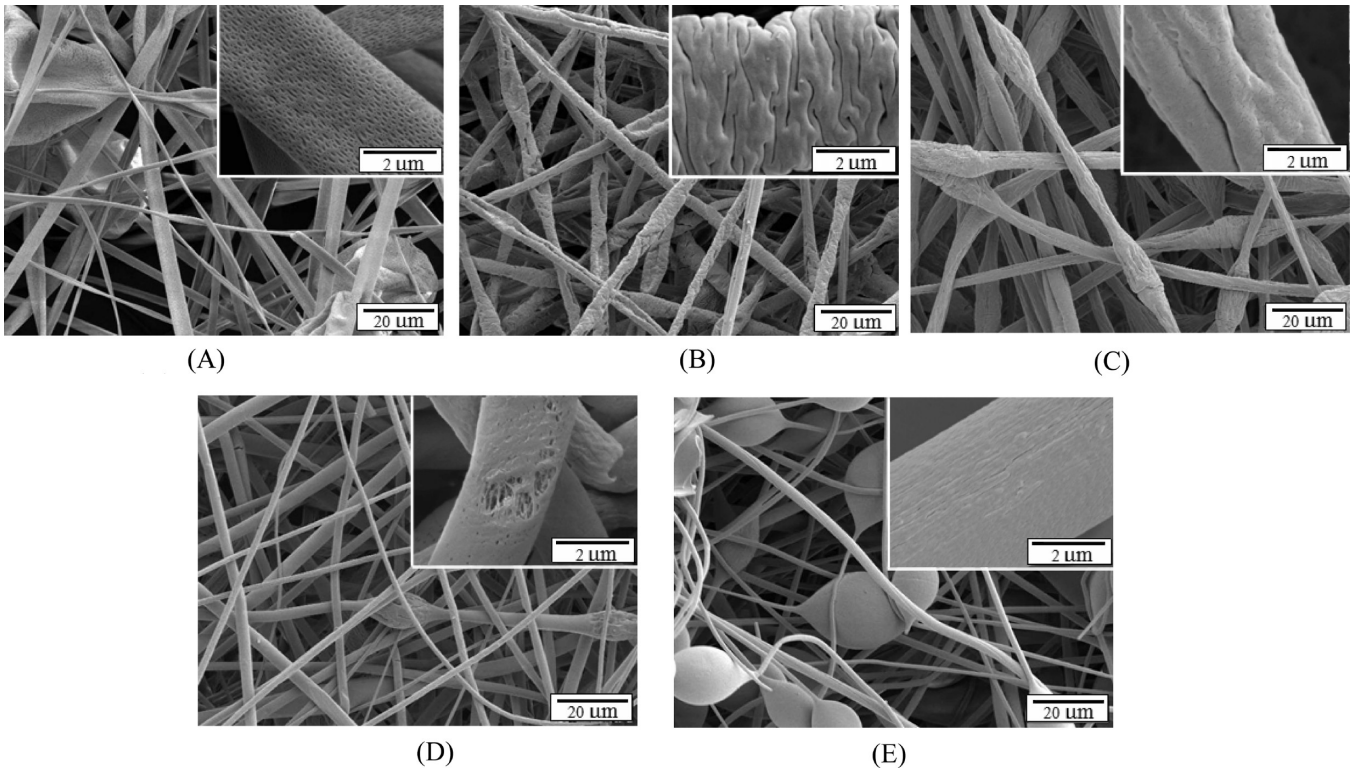

FIGURE 6. FE-SEM images of the PS fibers electrospun from 20 wt % PS solutions with different weight ratios of THF/DMF: (A) 4/0, (B) 3/1, (C) 2/2, (D) 1/3, and (E) 0/4.

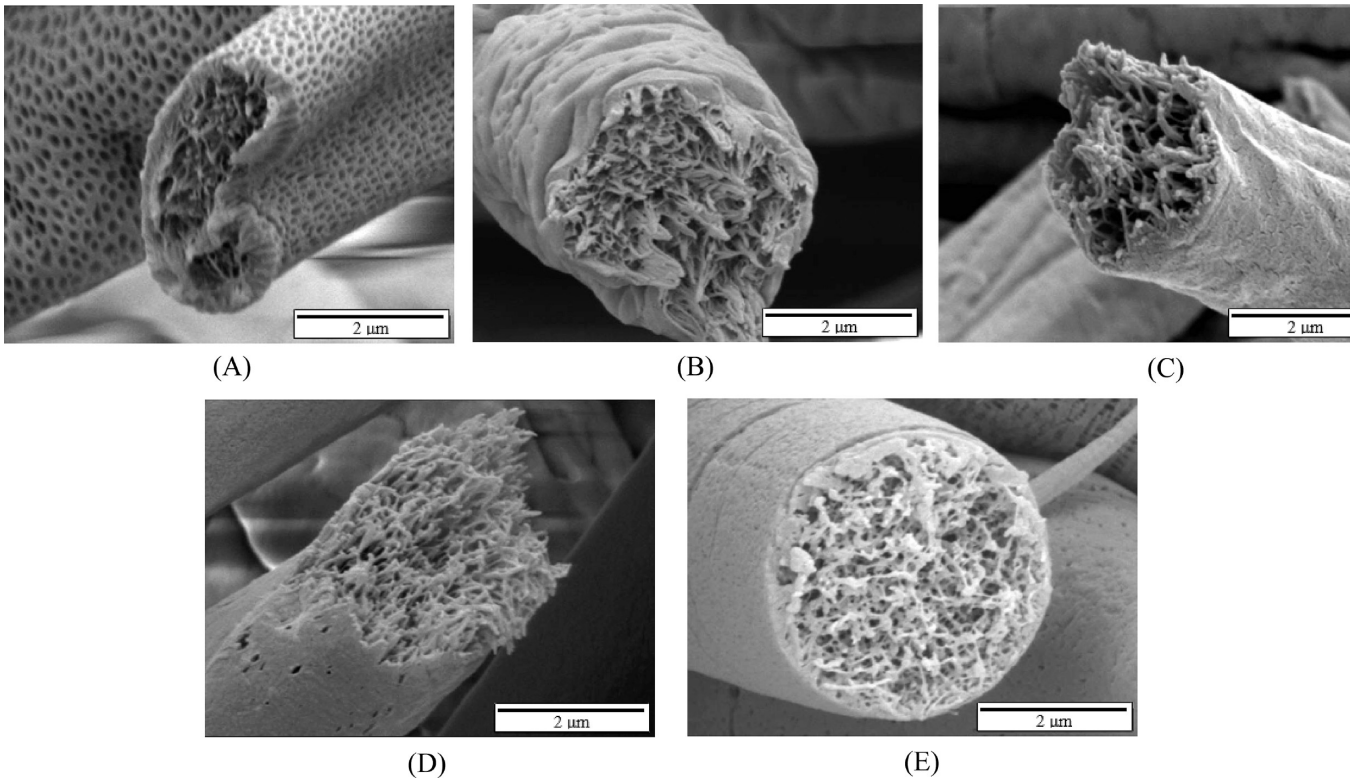

FIGURE 7. Cross-sectional FE-SEM images of PS fibers electrospun from 20 wt % PS solutions with different weight ratios of THF/DMF: (A) 4/0, (B) 3/1, (C) 2/2, (D) 1/3, and (E) 0/4.

electrical force. Simultaneously, the fiber collapsed more seriously as the polymer concentration decreased (Figures 6A and 2A). Previous studies showed that the more concentrated polymer solution, the stronger solvent retention ability (26). Therefore, the lower polymer concentration made the solvent easier to evaporate. As the solvent evaporated more quickly than the rate air and vapor penetrated into the fiber, the atmospheric pressure tended to collapse the fibers

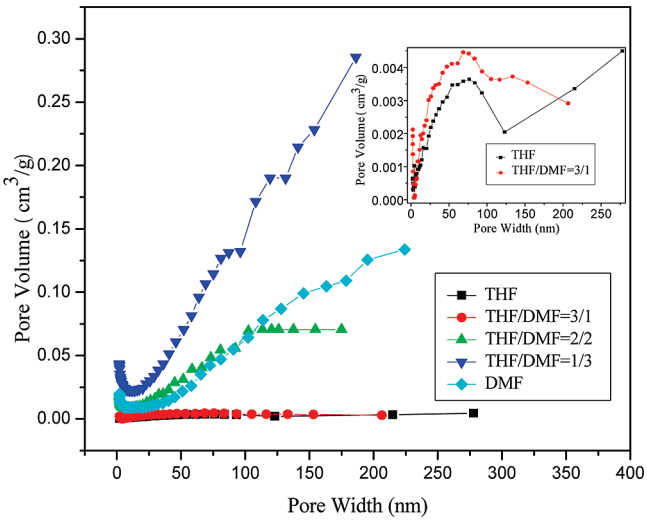

FIGURE 8. Pore size distribution for PS fibrous mats electrospun from 20 wt % PS solutions with different weight ratios of THF/DMF.

leading to the ribbonlike shape more seriously. Similar trends could also be seen from Figures 6B,C and 2B,C.

The FE-SEM images of the cross-sections of PS fibers electrospun from 20 wt % PS solutions showed more distinct porous structure (Figure 7) than those from the 30 wt % counterparts (Figure 3). PS fibers electrospun from THF with high vapor pressure were composed of the nanoporous sheaths and the inner three-dimensional (3D) interconnected nanofibrils along the fiber axis (Figure 7A). This observation of fiber morphology is different from another work (13), where the fibers were reported to be solid with densely packed pores on the surfaces of PS fibers also electrospun from THF only.

With increasing DMF content in the solvent mixtures, the 3D interconnected nanofibrils inside the fibers became thinner, the porous structure became more uniform and dense (Figure 7B–E). A comparison of Figure 7 with Figure 3 clearly illustrated that the interconnected nanofibrils inside the fiber became sparse, possibly because of the varying degrees of jet elongation resulting from the different solvent compositions and polymer concentrations in electrospinning.

The slightly reduced specific surface area of the fibers electrospun from the lower 20 wt % PS in THF alone is consistent with the observation of larger surface pores and lower pore volume (Figure 7A vs 3A and Figures 8 vs 4). Fibers generated at 20 wt % PS from all mixtures and DMF alone had much higher specific surface area than those electrospun from the 30 wt % PS solutions (Table 1). The specific surface area of the fibrous mats fabricated from the 20 wt % PS in 1/3 THF/DMF was 26.2 m^2 g^{-1}, nearly doubled.

It is well-known that various structures of electrospun PS nanofibers including beads can be obtained by tuning the polymer concentrations to induce the instable fluid jets formation (21, 27). The fibers formed from 10 wt % PS solutions exhibited beads-on-string morphology (Figure 9). The interesting finding was that with decreasing vapor pressure of the solvent mixtures, the fibrous mats transformed the collapsed-bead-dominant morphology into thin fibers with elliptical-bead-dominant morphology. Meanwhile, the size of beads was decreased. These phenomena could be attributed to the fluid jets instability resulting from the lower polymer concentration, high dielectric constant and conductivity solvent used in electrospining (28, 29). The

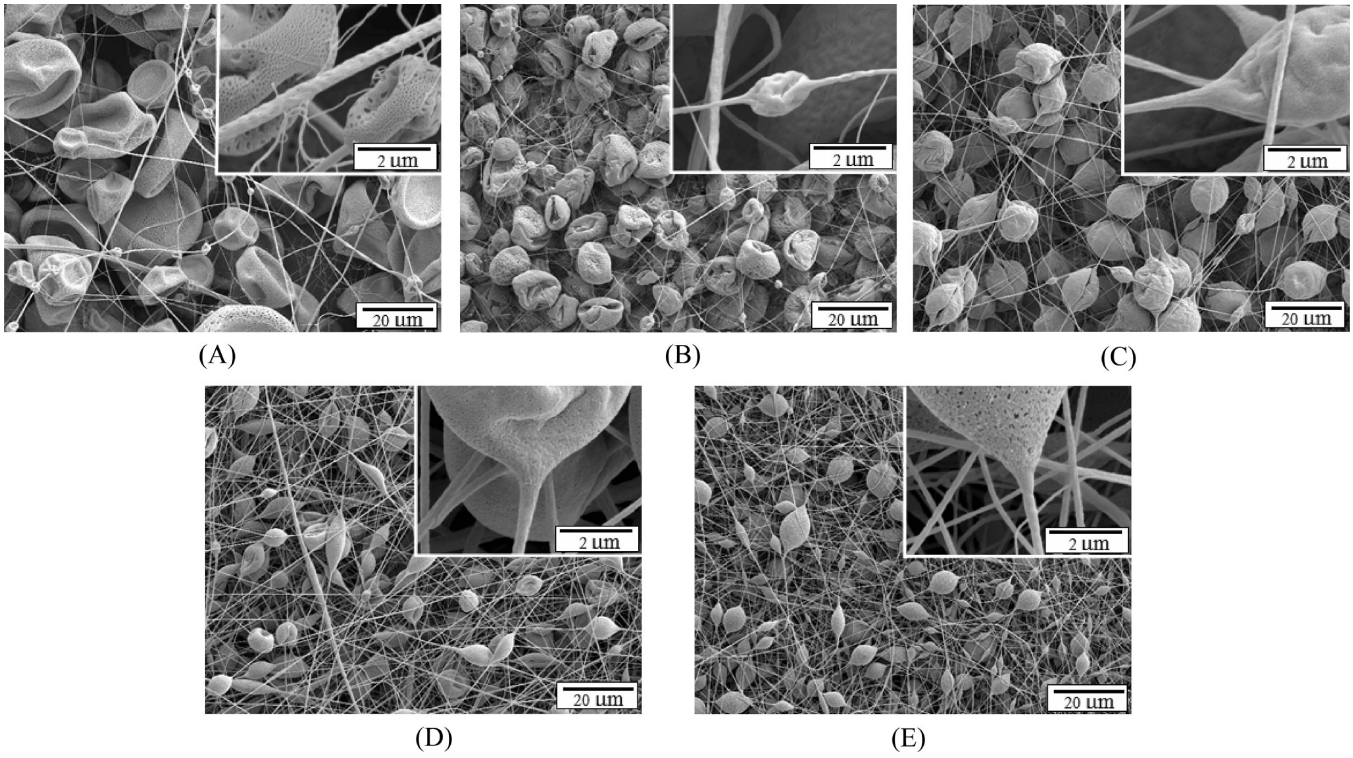

FIGURE 9. FE-SEM images of the PS fibers electrospun from 10 wt % PS solutions with different weight ratios of THF/DMF: (A) 4/0, (B) 3/1, (C) 2/2, (D) 1/3, and (E) 0/4.

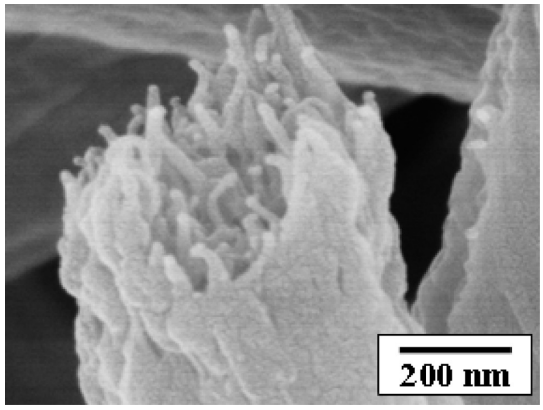

FIGURE 10. Cross-sectional FE-SEM image of PS fibers electrospun from a 10 wt % PS solution with a THF/DMF with a weight ratio of 1/3.

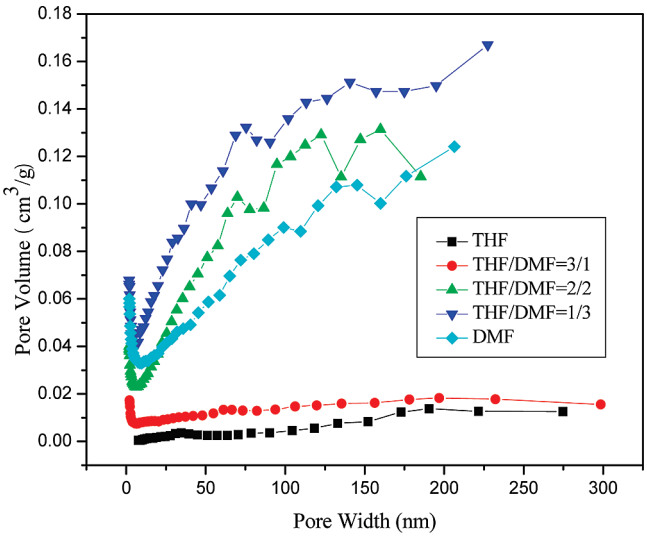

FIGURE 11. Pore size distribution for PS fibrous mats electrospun from 10 wt % PS solutions with different weight ratios of THF/DMF.

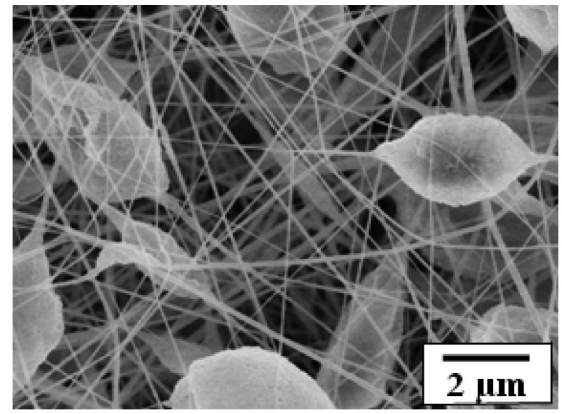

(A)

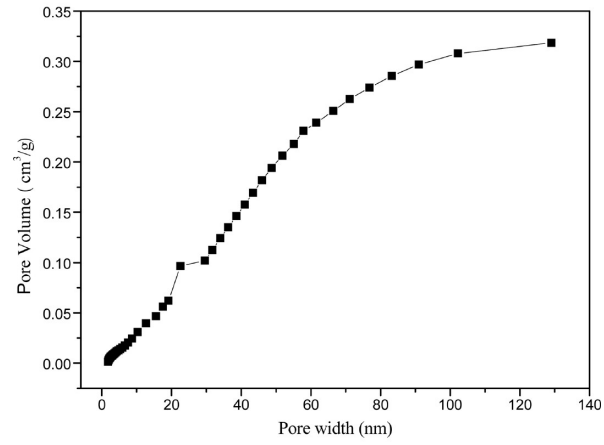

(B)

FIGURE 12. (A) FE-SEM image and (B) pore size distribution of PS fibers electrospun from a 5 wt % PS solution with a THF/DMF weight ratio of 1/3.

beads formation in electrospinning had been widely reported in many literatures (30−32). Figure 10 exhibited the cross-sectional FE-SEM image of sample shown in Figure 9D. It was found that the string fiber was highly porous comprising nanofibrils inside the fiber.

The pore size distribution for PS fibers electrospun from 10 wt % PS solutions with various solvent compositions is shown in Figure 11. It can be seen that the fibers formed with the THF/DMF weight ratios of 2/2, 1/3, and 0/4 possessed more pore volume with pore size below 100 nm compared with the concentrated samples shown in Figures 4 and 8. Fibers formed from the THF/DMF weight ratio of 1/3 had the largest specific surface area of 48.37 $m^2 g^{-1}$ and pore volume of 0.182 $cm^3 g^{-1}$, respectively. However, the beads-on-string fibers formed from THF alone showed the lowest specific surface area of 0.39 $m^2 g^{-1}$. Therefore, the formation of pores played the important role in increasing the specific surface area of fibers.

Figure 12 provided the morphology and pore size distribution of PS fibers formed from a 5 wt % PS solution with a THF/DMF weight ratio of 1/3. The sample still maintained the beads-on-string fiber structure as the sample formed from 10 wt % PS solution with same solvent composition, but thinner fiber diameter and smaller bead size. The prepared sample had the largest specific surface area of 54.92 $m^2 g^{-1}$ and pore volume of 0.318 $cm^3 g^{-1}$ among all samples.

CONCLUSIONS

Highly porous PS fibers have been directly prepared via electrospinning PS solutions by varying solvent compositions and polymer concentrations without the need for any post-treatment. The THF/DMF mixing ratio in PS solutions was proved to be the key parameter to affect porous structure induced by phase separation resulting from rapid evaporation of solvent in electrospinning. The high vapor pressure solvent THF created the fibers comprising nanoporous sheaths with 3D interconnected nanofibrils cores. As the vapor pressure of the solvent mixtures decreased, the micro- and nanoporous structures on the fiber surfaces disappeared but wrinkled or smooth surfaces presented, and the inner 3D interconnected nanofibrils became highly oriented. With decreasing PS concentration, the fiber diameters decreased and beads-on-string morphology emerged, providing even higher specific surface area and pore volume than those from a higher concentration. The fibrous mats electrospun

from 5 wt % PS in 1/3 THF/DMF showed largest specific surface area of 54.92 $m^2 g^{-1}$ and pore volume of 0.318 $cm^3 g^{-1}$, respectively. The ability to generate nanoporous polymer fibers with accurately controllable specific surface area and pore volume directly and in a simple one-step process will enhance their applicability significantly.

Acknowledgment. This work was partly supported by the National Natural Science Foundation of China under Grants 50803009 and 10872048. Partial support from the Program of Introducing Talents of Discipline to Universities (111-2-04 and B07024) is appreciated.

REFERENCES AND NOTES

(1) Doshi, J.; Reneker, D. H. *J. Electrostatics* **1995**, *35*, 151–160.
(2) Reneker, D. H.; Chun, I. *Nanotechnology* **1996**, *7*, 216–223.
(3) Zhu, Y. B.; Leong, M. F.; Ong, W. F.; Chan-Park, M. B.; Chian, K. S. *Biomaterials* **2007**, *28*, 861–868.
(4) Barhate, R. S.; Ramakrishna, S. *J. Membr. Sci.* **2007**, *296*, 1–8.
(5) Patel, A. C.; Li, S. X.; Wang, C.; Zhang, W. J.; Wei, Y. *Chem. Mater.* **2007**, *19*, 1231–1238.
(6) Ding, B.; Li, C. R.; Hotta, Y.; Kim, J. H.; Kuwaki, O.; Shiratori, S. *Nanotechnology* **2006**, *17*, 4332–4339.
(7) Li, X. H.; Ding, B.; Lin, J. Y.; Yu, J. Y.; Sun, G. *J. Phys. Chem. C* **2009**, *113*, 20452–20457.
(8) Tan, S. T.; Wendorff, J. H.; Pietzonka, C.; Jia, Z. H.; Wang, G. Q. *Chemphyschem* **2005**, *6*, 1461–1465.
(9) Wang, X. F.; Ding, B.; Yu, J. Y.; Wang, M. R.; Pan, F. K. *Nanotechnology* **2010**, *21*, 055502.
(10) Ding, B.; Wang, M. R.; Yu, J. Y.; Sun, G. *Sensors* **2009**, *9*, 1609–1624.
(11) Kokubo, H.; Ding, B.; Naka, T.; Tsuchihira, H.; Shiratori, S. *Nanotechnology* **2007**, *18*, 165604.
(12) Bognitzki, M.; Czado, W.; Frese, T.; Schaper, A.; Hellwig, M.; Steinhart, M.; Greiner, A.; Wendorff, J. H. *Adv. Mater.* **2001**, *13*, 70–72.
(13) Megelski, S.; Stephens, J. S.; Chase, D. B.; Rabolt, J. F. *Macromolecules* **2002**, *35*, 8456–8466.
(14) Casper, C. L.; Stephens, J. S.; Tassi, N. G.; Chase, D. B.; Rabolt, J. F. *Macromolecules* **2004**, *37*, 573–578.
(15) Miyauchi, Y.; Ding, B.; Shiratori, S. *Nanotechnology* **2006**, *17*, 5151–5156.
(16) Zhang, Y. Z.; Feng, Y.; Huang, Z. M.; Ramakrishna, S.; Lim, C. T. *Nanotechnology* **2006**, *17*, 901–908.
(17) Zhang, L. F.; Hsieh, Y. L. *Nanotechnology* **2006**, *17*, 4416–4423.
(18) Ji, L. W.; Saquing, C.; Khan, S. A.; Zhang, X. W. *Nanotechnology* **2008**, *19*, 085605.
(19) Gupta, A.; D.Saquing, C.; Afshari, M.; E.Tonelli, A.; A.khan, S.; Kotek, R. *Macromolecules* **2009**, *42*, 709–715.
(20) McCann, J. T.; Marquez, M.; Xia, Y. N. *J. Am. Chem. Soc.* **2006**, *128*, 1436–1437.
(21) Ji, Y.; Li, B. Q.; Ge, S. R.; Sokolov, J. C.; Rafailovich, M. H. *Langmuir* **2006**, *22*, 1321–1328.
(22) Wang, L. F.; Pai, C. L.; Boyce, M. C.; Rutledge, G. C. *Appl. Phys. Lett.* **2009**, *94*, 151916.
(23) Ziabicki, A. *Fundamentals of Fiber Formation*; Wiley: London, 1976.
(24) Arnauts, J.; Berghmans, H. *Physical Networks, Polymers and Gels*, Burchard, W.; Ross-Murphy, S B., Eds. Elsevier: New York, 1990; p 35.
(25) Kongkhlang, T.; Kotaki, M.; Kousaka, Y.; Umemura, T.; Nakaya, D.; Chirachanchai, S. *Macromolecules* **2008**, *41*, 4746–4752.
(26) Mark, H F.; Atlas, S M. Cernia, E. *Man-made Fibers Science and Technology*; Wiley: New York, 1967; Vol. 1, p 150.
(27) Fong, H.; Chun, I.; Reneker, D. H. *Polymer* **1999**, *40*, 4585–4592.
(28) Eda, G.; Liu, J.; Shivkumar, S. *Eur. Polym. J.* **2007**, *43*, 1154–1167.
(29) Uyar, T.; Besenbacher, F. *Polymer* **2008**, *49*, 5336–5343.
(30) Lee, K. H.; Kim, H. Y.; Bang, H. J.; Jung, Y. H.; Lee, S. G. *Polymer* **2003**, *44*, 4029–4034.
(31) Eda, G.; Shivkumar, S. *J. Mater. Sci.* **2006**, *41*, 5704–5708.
(32) Chen, H.; Snyder, J. D.; Elabd, Y. A. *Macromolecules* **2008**, *41*, 128–135.

AM900736H